Direct Power Control of a Three-Phase Inverter for Grid Input Current Shaping of a Single-Phase Diode Rectifier With a Small DC-Link Capacitor

Yeongrack Son, *Student Member, IEEE*, and Jung-Ik Ha, *Senior Member, IEEE*

***Abstract*—This paper describes motor drive system fed by a single-phase diode rectifier without power factor correction (PFC) circuit or the input filter. The system considered in this paper consists of a single-phase diode rectifier, a three-phase inverter, and a small dc-link capacitor. Since dc-link capacitance of the proposed system is few microfarads, the shape of the grid input current is directly affected by electrical output power of the inverter. Using this aspect, two goals of the drive system, controlling torque of the motor and suppressing the grid input current harmonics, can be simultaneously achieved by controlling the output power of the inverter. The proposed method includes the motor current reference generation and the direct output power regulation by modifying the output voltage reference. With the proposed method, the harmonic components of the grid input current can be reduced under the limits of the regulation IEC61000-3-2, lower than those in the conventional method. Also, the cost and size of the inverter system can be significantly reduced by removing electrolytic dc-link capacitor and input filter from the system. The performance of the proposed shaping method was validated by the experimental results using the motor drive system with a 5μF film capacitor at dc link.**

***Index Terms*—Direct power control, electrolytic capacitor, grid current harmonics reduction, pulse width modulation Inverters, small dc-link capacitor, variable speed drives.**

I. Introduction

RECENT advances in the power electronics technology have enabled variable-speed motor drives to be widely used for the low-power home applications, such as air conditioners, refrigerators, vacuum cleaners, etc. As shown in Fig. 1(a), the variable-speed motor drive for single-phase ac source is normally composed of a three-phase inverter, a single-phase diode rectifier, and a dc-link capacitor. In general, the dc-link capacitance is designed as a high value so that the system maintains a constant dc-link voltage. The electrolytic capacitor has high capacitance per volume, so it is widely used as the dc-link capacitor to reduce the volume of the system. However, the electrolytic capacitor has some drawbacks. First, since the electrolyte included in this capacitor evaporates, it is vulnerable to the current ripple and the heat. Due to this characteristic, the electrolytic capacitor for the dc link has about thousand hours of the lifetime at 105 °C, and the lifetime reduces to half for every 10 °C of the temperature rise [2]. Because of its short lifetime, the electrolytic capacitor critically affects the reliability of the drive circuit; about 60% of the drive circuit failures are due to the electrolytic capacitor [2]–[8]. Another problem is that the conventional drive is hard to satisfy the regulation about the grid input current harmonics. Nonlinear grid input current is inevitable due to the constant dc-link voltage, as shown in Fig. 1(b) [9]–[13]. These current harmonics increase the stress on low-voltage ac grid and lower the grid quality, so the regulations on the harmonic grid input current are introduced and all electrical equipment connected to the grid should comply with the regulations [1]. To make the drive with electrolytic dc-link capacitor satisfy the regulation, inductive line filter or power factor correction (PFC) circuit is needed to reduce the current harmonics [14]–[18]. These circuits increase the cost and the volume of the drive [19].

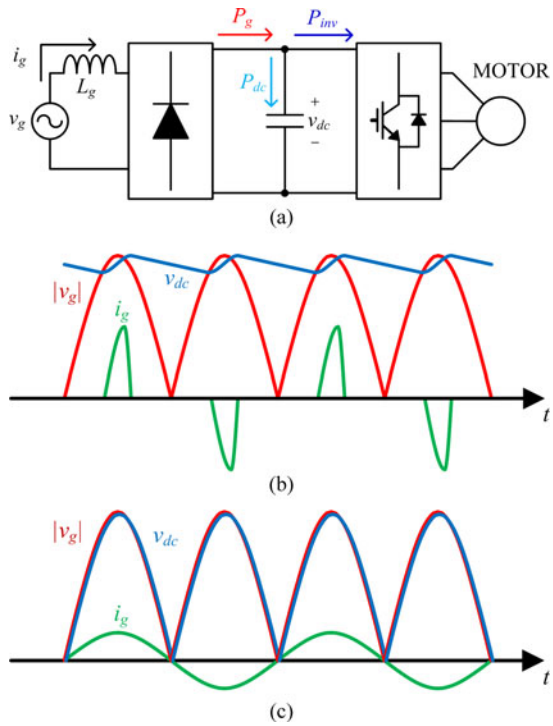

Fig. 1. Variable-speed motor drive with the single-phase diode rectifier. (a) Circuit diagram. (b) Waveforms of $|v_g|$, i_g, and v_{dc} with electrolytic dc-link capacitor. (c) Waveforms of $|v_g|$, i_g, and v_{dc} without electrolytic dc-link capacitor.

Manuscript received October 23, 2013; revised March 9, 2014 and May 24, 2014; accepted July 18, 2014. Date of publication August 5, 2014; date of current version February 13, 2015. This work was supported by the National Research Foundation of Korea (NRF) Grant funded by the Ministry of Science, ICT, & Future Planning (MSIP) (2009-0083495) and the Brain Korea 21 Plus Project in 2014. Recommended for publication by Associate Editor P. C. Loh.

The authors are with the Department of Electrical and Computer Engineering, Seoul National University, Seoul 151-742, Korea (e-mail: syrident@snu.ac.kr; jungikha@snu.ac.kr).

Color versions of one or more of the figures in this paper are available online at http://ieeexplore.ieee.org.

Digital Object Identifier 10.1109/TPEL.2014.2345421

The motor drive with low capacitance in dc link has been developed to overcome these drawbacks of the electrolytic capacitor [20]–[25]. This kind of the drive has the dc-link capacitance lower than 1% of the capacitance in the conventional drive so that the dc-link voltage fluctuates and the diode rectifier conducts continuously, as shown in Fig. 1(c) [26]–[28]. In this case, the capacitor with low capacitance per volume, such as a film capacitor or a ceramic capacitor, can be used in dc link of the drive. Since these kinds of capacitor allow large ripple current and have much longer lifetime than the electrolytic one, the reliability of the drive circuit can be improved [25]. The manufacturing cost of the drive is also reduced by using the film or ceramic capacitor in dc link. It is because the film capacitor is cheaper than the electrolytic one and the line filter can be lightened by lowering the dc-link capacitance. In the motor drive with 1 kW power rating, the manufacturing cost per unit of the drive, which includes the cost of dc-link capacitor and line filter is reduced about $10 by using the film or ceramic dc-link capacitor. Because of the low dc-link capacitance, there is a drawback of the drive without electrolytic capacitor; the ride-through capability of the drive is below 1% of the conventional drive. So the proposed motor drive cannot be applied to the application in which the ride-through capability is important. However, the ride-through capability is not a key factor in the low-power and low-performance application. Several major appliance companies use this feature and present the products with film capacitor in the market. The proposed scheme is also researched for such applications.

In the motor drive without electrolytic capacitor, the output power of the inverter should be precisely controlled to suppress the grid input current harmonics. In order to make the sinusoidal grid input current, many motor control methods for the drive without electrolytic capacitor has been researched [20]–[22]. But it is hard for them to suppress the harmonics exactly because of improper consideration about the inverter output power in motor current reference, low bandwidth of the controllers, and the motor current control error by fluctuating dc-link voltage.

In this paper, a novel grid input-current-shaping method for the drive without electrolytic capacitor is proposed. The design criterion of the dc-link capacitor in the drive circuit is presented in Section II. The conditions for the sinusoidal grid input are introduced in Section III. The proposed grid-input-current-shaping method, including the stability analysis of the system is explained in Section IV. The experimental results for validating the improvements of the proposed method are in Section V.

II. Design Consideration of a DC-Link Capacitor

In general, the dc-link voltage ripple and the capacitor current ripple are the main design considerations of the dc-link capacitor. In case that the electrolytic capacitor is used as dc-link capacitor, the capacitance is designed so that the current ripple through the capacitor is maintained below the ripple current limit of the capacitor. The dc-link voltage fluctuation by change of the load is also taken into account [29]. Normally, about 680 μF electrolytic capacitor with the ripple current rating of 3–4 A and the dc voltage limit of 400–450 V can be used in the motor drive with 1 kW power rating. Here, the value is determined by the ripple current because the switching ripple voltage and the load fluctuation are very low. On the other hand, where a film or a ceramic capacitor is used, the current ripple limit is not so critical. The limitations of the design are the switching ripple and the load fluctuation in dc-link voltage. Since the energy of load fluctuation is higher than that of switching ripple, the applications without any load fluctuation should be considered for the inverter system with the small dc-link capacitor. Finally, the switching ripple voltage can be only the design criterion. The load fluctuations can be suppressed by the control in the applications of air conditioner, pump, compressor, etc. Therefore, the small dc-link capacitor configurations have been considered and commercialized only for these applications.

The large voltage ripple can reduce the voltage for the motor control, generate the electromagnetic noises, or make the low conversion efficiency, so keeping the switching ripple of the dc-link voltage under certain limit is important. In this paper, a 5 μF film capacitor is used as a dc-link capacitor so that the switching ripple at rated power is below 10% of the dc-link voltage peak. By using a film capacitor, over 99% of the capacitance is reduced in comparison with the electrolytic capacitor drive.

III. Conditions for Sinusoidal Grid Input Current

Assuming that the voltage drop in diode rectifier is ignorable, the relationship between the grid input current and the dc-link voltage in positive v_g case is defined as follows:

$$v_g - v_{\rm dc} = R_g i_g + L_g \frac{di_g}{dt} \tag{1}$$

where R_g and L_g are the grid resistance and inductance, including line filter impedance. Fig. 1(b) and (c) shows the waveforms of v_g, v_{dc}, and i_g in the drive with electrolytic capacitor and in the drive without electrolytic capacitor. The relationship in negative v_g can be expressed from (1) by changing v_g to $-v_g$. The shape of dc-link voltage when sinusoidal grid input current flows into the drive is calculated from (1). In case of the proposed motor drive, R_g and L_g are so small that they can be ignored. Therefore, where the grid voltage is sinusoidal, the shape of dc-link voltage for sinusoidal grid input current is expressed as follows:

$$\begin{aligned} v_{\rm dc} = \; & V_g \sin\theta_g + R_g I_g \sin\theta_g \\ & + L_g \frac{d}{dt}(I_g \sin\theta_g) \approx |V_g \sin\theta_g| \end{aligned} \tag{2}$$

where V_g and I_g are zero-to-peak amplitudes of the grid voltage and current, respectively, and θ_g is the phase angle of the grid. The diode rectifier, which is passively turned on and off, has no factor to control the power of the grid side and the dc-link voltage. Since the output power of the inverter is the only factor which can control the dc-link voltage, the shape of the output power should be exactly determined to make the dc-link voltage as (2). Where the grid input current is sinusoidal, the input power from the grid is given by

$$P_g = |v_{\rm dc}|\,|i_g| = |V_g \sin\theta_g|\,|I_g \sin\theta_g| = V_g I_g \sin^2(\theta_g). \tag{3}$$

Here, the electric power by fluctuating dc-link voltage is calculated as

$$P_{\rm dc} = v_{\rm dc} \cdot C_{\rm dc} \frac{dv_{\rm dc}}{dt} = \frac{1}{2}\omega_g C_{\rm dc} V_g^2 \sin(2\theta_g) \tag{4}$$

where C_{dc} is the capacitance of the dc-link capacitor and ω_g is angular speed of the ac grid. As in (5), the output power of the inverter $P_{\rm inv}$ with sinusoidal grid input current is calculated by subtracting (4) from (3). In other words, $P_{\rm inv}$ is controlled as follows in order to obtain the sinusoidal grid input current of the motor drive:

$$P_{\rm inv} = P_g - P_{\rm dc} = V_g I_g \sin^2(\theta_g) - \frac{1}{2}\omega_g C_{\rm dc} V_g^2 \sin(2\theta_g). \tag{5}$$

The output power of the inverter is determined by the inner product of the motor current vector and the motor voltage vector, as in (6). Using the *d–q* voltage equation (7) of the IPM in the synchronous reference frame, (6) is derived as the sum of the mechanical power of the motor, the conduction loss of the motor, and the inductive power by change of the motor current, as in (8)

$$P_{\rm inv} = 1.5(\vec{v}_{dq} \cdot \vec{i}_{dq}) = 1.5(v_d i_d + v_q i_q) \tag{6}$$

$$\begin{aligned} v_d &= R_s i_d + L_d \frac{di_d}{dt} - \omega_r L_q i_q \\ v_q &= R_s i_q + L_q \frac{di_q}{dt} + \omega_r (L_d i_d + \lambda_f) \end{aligned} \tag{7}$$

$$\begin{aligned} P_{\rm inv} &= 1.5\omega_r i_q \{\lambda_f + (L_d - L_q) i_d\} \\ &\quad + 1.5 R_s (i_d^2 + i_q^2) + 1.5 \left(L_d i_d \frac{di_d}{dt} + L_q i_q \frac{di_q}{dt} \right) \\ &= P_m + P_{\rm loss} + P_{\rm ind} \end{aligned} \tag{8}$$

where v_d, v_q, i_d, i_q, R_s, L_d, L_q, λ_f, and ω_r are voltages and currents of the motor in arbitrary *d–q* reference frame, the stator resistor, the *d–q* axis inductors, the flux by the permanent magnet of the motor, and the angular speed of the motor.

One more thing to be considered for regulating v_{dc} as in (2) is the output voltage of the inverter. In case that the motor connected to the drive is operated at high speed, the line-to-line voltage of the motor can be higher than the dc-link voltage. This leads to the energy generation and rise of the dc-link voltage. In order to prevent them, the amplitude of the inverter output voltage reference $|v^*_{\rm out}|$ is controlled to be lower than or equal to the output voltage limit of the inverter, as shown

$$|v^*_{\rm out}| \equiv \sqrt{(v^*_d)^2 + (v^*_q)^2} \le V_{\rm lim} \approx \frac{|V_g \sin(\theta_g)|}{\sqrt{3}} \tag{9}$$

where v^*_d and v^*_q are the output voltage references of the inverter in arbitrary *d–q* reference frame, respectively.

IV. Proposed Grid-Input-Current-Shaping Method

The block diagram of the proposed method is shown in Fig. 2. The current reference generator and the output power controller are added to the cascaded speed and current controllers, and overmodulation method considering the dc-link fluctuation is proposed. In the proposed method, fast grid-input-current-shaping can satisfy (5) and (9).

A. Generation of the Reference

The peak amplitude of the current I_g in (5) is determined by the mechanical power of the motor

$$P^*_{\rm inv} \approx 2\omega_{\rm rm} T^*_e \sin^2(\theta_g) - 0.5\omega_g C_{\rm dc} V_g^2 \sin(2\theta_g) \tag{10}$$

where ω_{rm} and T^*_e are the rotational speed and the torque reference of the motor. As the amounts of $P_{\rm loss}$ and $P_{\rm ind}$ in (8) are considered, I_g becomes larger than the calculated one. Here, in order to find out the grid angle θ_g, the fluctuating v_g or v_{dc} is used as input of the phase-locked loop (PLL) block in Fig. 2.

In the *d–q* current reference generation, (9) and (10) are expressed as (11) and (12), represented with the *d–q* currents of the motor

$$\begin{aligned} &1.5\omega_r i_q \{\lambda_f + (L_d - L_q) i_d\} + 1.5 R_s (i_d^2 + i_q^2) \\ &+ 1.5 \left(L_d i_d \frac{di_d}{dt} + L_q i_q \frac{di_q}{dt} \right) \approx 2\omega_{rm} T^*_e \sin^2(\theta_g) \\ &- 0.5\omega_g C_{dc} V_g^2 \sin(2\theta_g) \end{aligned} \tag{11}$$

By solving (11), and (12) as shown at the bottom of the page, the *d–q* current waveforms that satisfy both conditions can be calculated. However, because the conditions have nonlinear terms, it needs the complicated algorithm and long time to obtain accurate solutions. To solve them easily and fast, the proposed motor current reference generation method approximately calculates the motor current reference. The approximated *d–q* current waveform using Fourier series is presented as follows:

$$\begin{aligned} i_d &= I_{d,0} + \sum_{k=1}^{\infty} I_{d,k} \sin(2k\theta_g + \phi_{d,k}) \approx I_{d,0} \\ &\quad + \sum_{k=1}^{n} I_{d,k} \sin(2k\theta_g + \phi_{d,k}) \\ i_q &= I_{q,0} + \sum_{k=1}^{\infty} I_{q,k} \sin(2k\theta_g + \phi_{q,k}) \approx I_{q,0} \\ &\quad + \sum_{k=1}^{n} I_{q,k} \sin(2k\theta_g + \phi_{q,k}) \end{aligned} \tag{13}$$

where $I_{d,k}$, $I_{q,k}$, $\phi_{d,k}$, and $\phi_{q,k}$ are the zero-to-peak amplitudes and the phases of kth harmonic components of the *d–q*

$$\sqrt{\left(R_s i_d + L_d \frac{di_d}{dt} - \omega_r L_q i_q \right)^2 + \left\{ R_s i_q + L_q \frac{di_q}{dt} + \omega_r (L_d i_d + \lambda_f) \right\}^2} \le \frac{|V_g \sin(\theta_g)|}{\sqrt{3}} \tag{12}$$

.

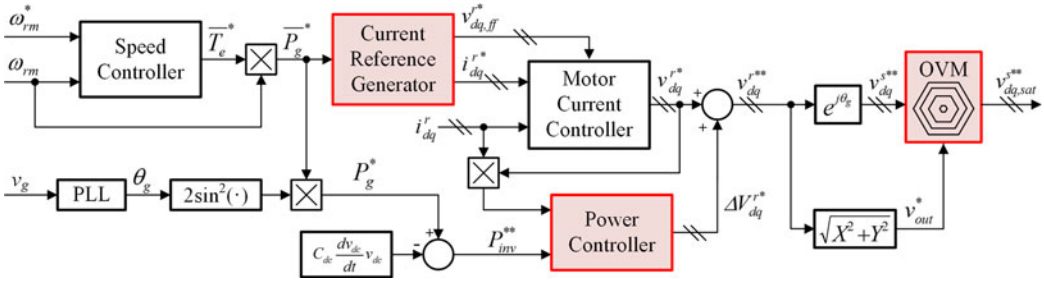

Fig. 2. Overall block diagram of the proposed grid-input-current-shaping method.

currents, respectively. Since P_{inv} and v_{dc} fluctuate with twice the grid frequency, the fundamental one of the Fourier series is defined as this frequency. The value of *n* is determined in considering the bandwidth of the motor current controller. If *n* is big, the reference has harmonic components at the high frequency and they cannot be controlled due to the limited bandwidth. In opposite case, if *n* is small, the output power from the approximated current reference has a big error with the output power reference in (10).

The reference calculation process is as follows. First, one case of the *d–q* current waveforms can be determined as (13) by setting the amplitude variables and the angle ones. In this step, $I_{d,0}$ and $I_{q,0}$ are selected to satisfy the torque reference. The output power error and the margin of the output voltage can be found by substituting them to (11) and (12). By changing the variables and repeating the process mentioned earlier, the solution of two conditions that minimizes these errors can be derived. Fig. 3 describes the example of the current reference generation. It can be found that the calculated current reference approximately satisfies both (11) and (12). A lot of computation time is required to search the coefficients in (13), which satisfy (11) and (12). It is hard to finish this calculation in single sampling period, so the references at several operating points are calculated in off-line and saved as the lookup table.

In the motor current controller, feed-forward voltage reference is used to compensate the effect of the back electromotive force (EMF). Since both *d–q* currents of the motor can fluctuate, the compensation of the feed-forward voltage reference is more important in the proposed motor drive case. The *d–q* feed-forward voltage references are expressed as follows:

$$\begin{aligned} v^*_{d,ff} &= -\omega_r L_q i^*_q \\ v^*_{q,ff} &= \omega_r (L_d i^*_d + \lambda_f). \end{aligned} \tag{14}$$

Since the output power of the inverter fluctuates as twice of the grid frequency, the components of $n = 0$ and $n = 1$ are dominant in (13). To regulate the motor current as the fluctuating reference with minimizing the control delay, the bandwidth of the motor current controller is designed sufficiently higher than the dominant frequency of the reference [30]–[33]. The closed-loop gain of the motor control system, including the PI current controller and the motor plant is shown as follows:

$$\frac{i}{i^*} = \frac{k_p + (k_i/s)}{(sL + R + k_p + (k_i/s))}$$

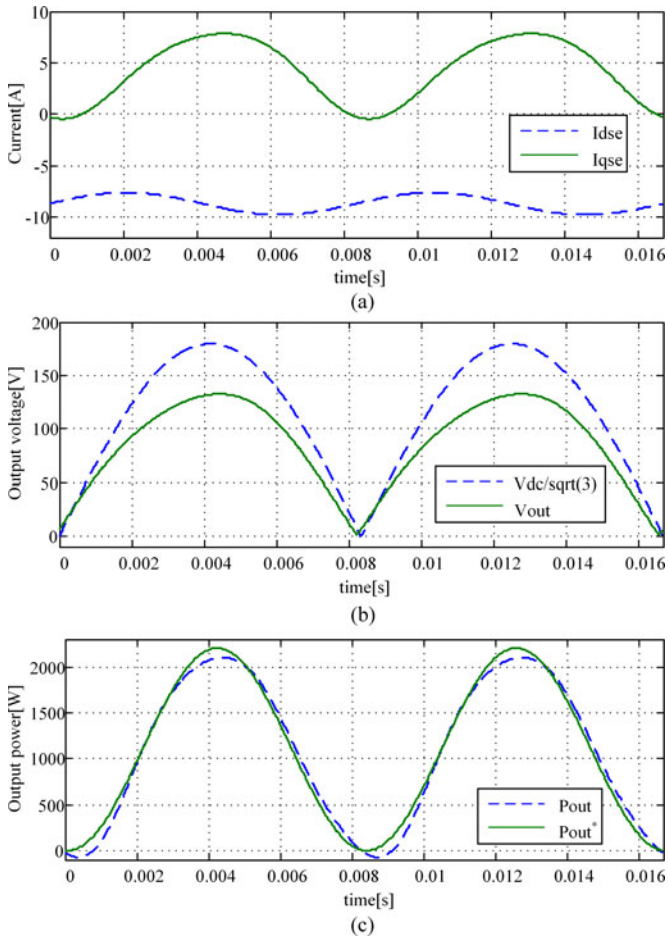

Fig. 3. Example of motor current waveforms. (a) *d–q* currents. (b) Output voltages. (c) Output power of the inverter.

$$= \frac{L\omega_{cc} + (R\omega_{cc}/s)}{(sL + R + L\omega_{cc} + (R\omega_{cc}/s))} = \frac{\omega_{cc}}{s + \omega_{cc}} \tag{15}$$

where *R*, *L*, and ω_{cc} are the resistance of the motor, the inductance of the motor, and the bandwidth of the PI current controller, respectively. The discrete switching effect can be ignored because the switching frequency is much higher than the magnitudes of the negatives poles in (15). In this paper, the bandwidth of the motor current controller is set as 600 Hz. With this bandwidth, the phase delay at $s = 120$ Hz is about 10°.

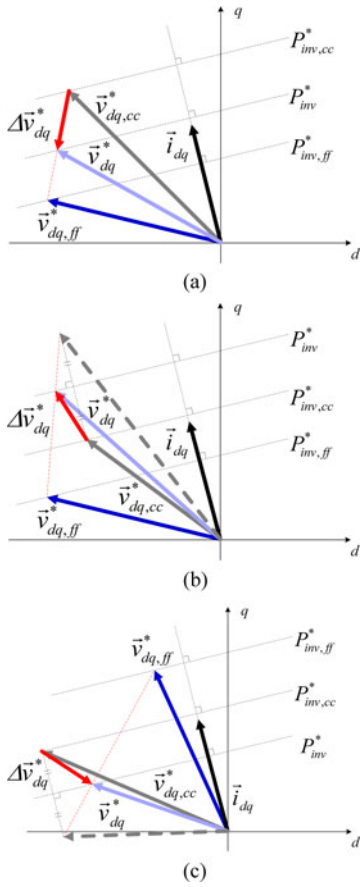

Fig. 4. Vector diagram of the voltage modification for the output power control. (a) $P^*_{inv,cc} < P^*_{inv} < P^*_{inv,ff}$ or $P^*_{invff} < P^*_{inv} < P^*_{inv,cc}$. (b) $P^*_{inv} > P^*_{inv,cc}$ and $P^*_{inv} > P^*_{inv,ff}$. (c) $P^*_{inv} < P^*_{inv,cc}$ and $P^*_{inv} < P^*_{inv,ff}$.

B. Direct Inverter Output Power Control by Voltage Reference Modification

The grid input current harmonics cannot be suppressed exactly only by the motor current control with *d–q* current references aforementioned, since the current controller with low bandwidth cannot follow the high order reference. The current controller also cannot reject the high-frequency resonant currents between line inductance and dc-link capacitor, since the resonant frequency of the drive without electrolytic capacitor is usually higher than the bandwidth of the current controller. The proposed motor drive is a voltage-source inverter (VSI) type, and it can generate the output voltage as the reference in a single switching period [34]. Therefore, with the direct control of the inverter output power by output voltage control, the output power of the inverter can follow the reference more correctly and faster than the conventional methods using motor current control.

In case that the output power calculated with the motor current vector and the output voltage reference vector from the current controller is not equal to the output power reference in (10), the voltage reference vector is modified to compensate the difference. Since the voltage reference modification can affect the performance of the current controller and the dynamics of the motor current, the strategy to minimize these effects is needed. Fig. 4 shows the vector diagram of the proposed output voltage reference modification. In Fig. 4, $\vec{v}^*_{dq,cc}$, $\vec{v}^*_{dq,ff}$, $\vec{v}^*_{dq}$, $\Delta\vec{v}^*_{dq}$, and $\vec{i}_{dq}$ are the *d–q* voltage reference from the current controller, the *d–q* feed-forward voltage reference, the final output voltage reference, and the *d–q* current vector, respectively. The dashed line perpendicular to the current vector is the trace of the voltage vectors which generate the output power. $P^*_{\mathrm{inv},cc}$, $P^*_{\mathrm{inv},ff}$, and P^*_{inv} are the output power references calculated from $\vec{v}^*_{dq,cc}$,$\vec{v}^*_{dq,ff}$, and$\vec{v}^*_{dq}$, respectively. Fig. 4(a) shows the case that $P^*_{\mathrm{inv}}$is located between $P^*_{\mathrm{inv},cc}$ and $P^*_{\mathrm{inv},ff}$. In this vector diagram, $\Delta\vec{v}^*_{dq}$ means the voltage disturbance to the current controller and $\vec{v}^*_{dq} - \vec{v}^*_{dq,ff}$ is the dynamic voltage component, which is related to the motor current dynamics. The motor current can be increased where $\vec{v}^*_{dq} - \vec{v}^*_{dq,ff}$ is large. $\vec{v}^*_{dq} - \vec{v}^*_{dq,ff}$ should be small for the stable motor current control. Hence, the voltage reference is modified along the shortest path from $\vec{v}^*_{dq,cc}$ to $\vec{v}^*_{dq,ff}$ through P^*_{inv} line in the proposed method. This voltage modification strategy can minimize the effects on the motor control. The output voltage reference is modified in the same manner in the case that P^*_{inv} is larger or smaller than both $P^*_{\mathrm{inv},cc}$ and$P^*_{\mathrm{inv},ff}$, as shown in Fig. 4(b) and (c). The modified voltage in these cases are selected as the ones with the shortest distance between $\vec{v}^*_{dq}$ and $\vec{v}^*_{dq,ff}$, based on the dashed line.

By applying the voltage modification method, the bandwidth of the power controller is widened to about half of the switching frequency. Therefore, the high-frequency currents by the resonance can be suppressed, and the output power error can be reduced without controlling the high order current reference. Also, the voltage modification to the back-EMF vector can minimize the effect on the current regulation performance [35].

C. Overmodulation Method With Maintenance of Output Power

In case that magnitude of the output voltage reference is over the output voltage limit of the inverter, overmodulation method is applied so that the output voltage reference is reduced into the output voltage limit. There is no consideration on the output power of the inverter in the conventional overmodulation method [35]–[41], so the output power can be changed after the voltage reference is limited by overmodulation. This output power error can distort the grid input current, so the strategy to keep the output power of the inverter during overmodulation is needed. The proposed overmodulation method limits the output voltage reference along the dotted line so that inner product of the motor current vector and the output voltage reference after modification has the same value. The output voltage limitation to the other sector can be accepted to keep the output power. The implementation of the proposed overmodulation method is more difficult than the conventional one, since several vector calculations are needed to get the limited output voltage reference. Fig. 5 represents an example of the proposed overmodulation method.

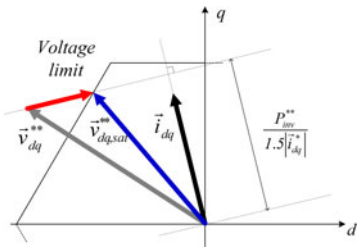

Fig. 5. Vector diagram of the voltage modification for the proposed overmodulation method.

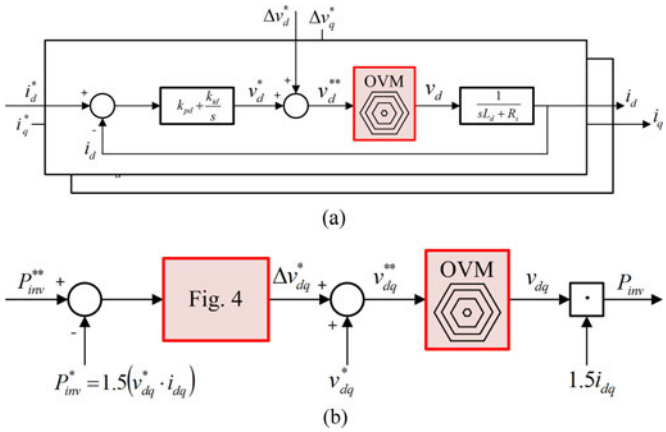

Fig. 6. Control Block diagrams. (a) Motor current control loop. (b) Output power control loop.

D. Stability Analysis of the Proposed Motor Drive System

The stability of the proposed system is analyzed in two aspects: the stability of the motor current control system and the stability of the grid current control system. Brief control loop of two systems are shown in Fig. 6. First, in the motor current controller as shown in Fig. 6(a), the output of the inverter output power controller acts as a disturbance. Assuming that the nonlinear effect of the overmodulation is negligible, the d-axis current response due to this disturbance is shown as follows:

$$\left.\frac{i_d}{\Delta v_d^*}\right|_{i_d^*=0} = \frac{1}{R_s + sL_d + k_{pd} + (k_{id}/s)} = \frac{1}{L_d}\frac{s}{(s + (R_s/L_d))(s + \omega_{cc})} \tag{16}$$

where k_{pd} and k_{id} are the gains of the d-axis PI current controller. In this transfer function, it can be seen that the function is stable since the number of poles is larger than the number of zeros and all of the poles are negative. In (16), same as in (15), the switching effect is ignored. The q-axis current response is also stable because the q-axis current controller has same structure with the d-axis current controller. Therefore, it can be found that the effect of the power controller on the motor current converges to zero.

As shown in Fig. 6(b), since the proposed power controller directly compensates the output power error through the feed-forward loop, the control loop gain is 1 where the overmodulation effect and the discrete sampling effect are neglected. In other words, all of the grid current harmonics including the one by LC resonance of the line filter and the dc-link capacitor can be correctly regulated through the proposed power controller. However, the grid current control loop gain is asymptotically shown as the first low-pass filter, when the influence of the sampling effect is considered. The control loop gain of the power controller considering the sampling effect is shown as follows:

$$\frac{P_{\rm inv}}{P_{\rm inv}^{**}} = \frac{1.5(v_{dq}\cdot i_{dq})}{1.5(v_{dq}^{**}\cdot i_{dq})} = \frac{v_{dq}}{v_{dq}^{**}} = \frac{1}{1+sT_d} \tag{17}$$

$$\frac{i_g}{i_g^*} = \frac{P_g}{P_g^*} = \frac{P_{\rm inv}+P_{\rm dc}}{P_{\rm inv}^{**}+P_{\rm dc}} \cong \frac{1}{1+sT_d} \tag{18}$$

where T_d is the delay time due to the sampling effect. It can be found that the grid inductance L_g should be designed so that the resonant frequency is lower than the cutoff frequency of the power controller and the proposed controller can suppress the resonant components of the grid current. In this paper, designed L_g including the line inductance is 300 μH. The resonant frequency with 300 μH L_g is about 4 kHz, which is lower than half of the switching frequency.

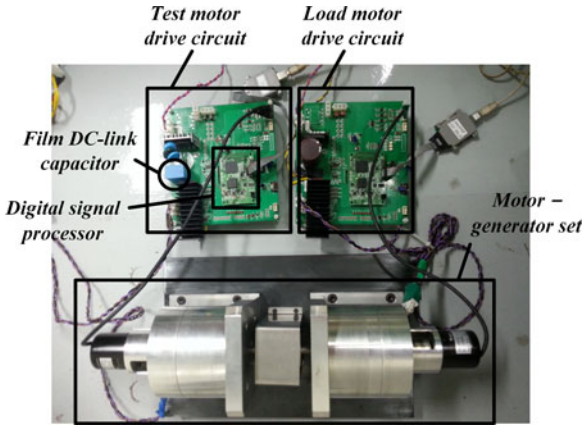

Fig. 7. Experimental hardware configuration.

V. Experimental Result

Experiments are performed to verify the performance of the proposed grid-input-current-shaping method. Experimental hardware is configured as in Fig. 7. The test motor is a 1-kW IPMSM, and the proposed controller is implemented with TI digital signal processor (DSP) TMS320C28346. The power meter VOLTECH PM6000 is used to measure the grid current harmonics and compare with the regulation. The parameters of the experimental hardware are listed in Table I.

The grid-input-current-shaping performance with conventional cascaded speed–current controller is shown in Fig. 8. The load machine is controlled as the rated speed and the average torque of the test motor is controlled as the rated torque. Each waveform from top to bottom shows the grid input current, the dc-link voltage, the q-axis current, and the d-axis current of the

TABLE I
PARAMETERS OF THE EXPERIMENTAL SYSTEM

Parameter	Values
Rated power	1 kW
Rated speed	3600 r/min
Rated torque	2.65 N · m
Stator resistance	1.09 Ω
d-axis/*q*-axis inductance	8.77 mH/12.87 mH
Back-EMF constant	0.0947 V · s/rad
Number of poles	6
DC-link capacitance	5 μF
Line filter inductance	300 μH
Grid voltage	220 Vrms
Grid frequency	60 Hz
Switching frequency	10 kHz
Sampling frequency	10 kHz

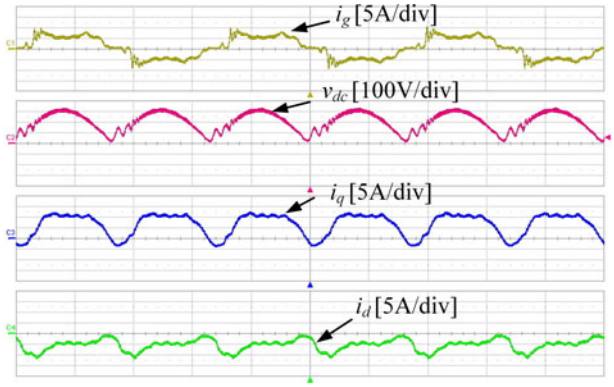

Fig. 8. Waveforms of the motor drive with the conventional cascaded speed–current controller.

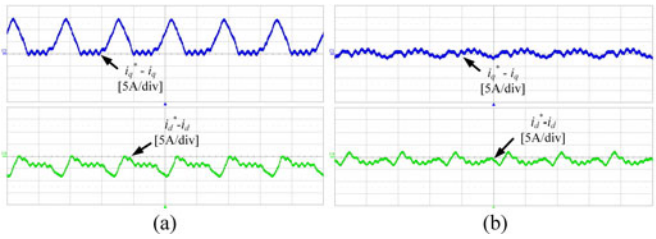

Fig. 9. *d–q* axis current control errors: (a) in the constant current reference; (b) in the reference generated by the proposed current reference generation method.

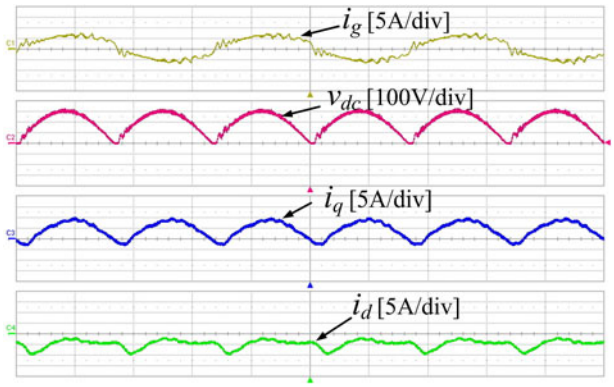

Fig. 10. Waveforms of the motor drive with the proposed current reference generation method.

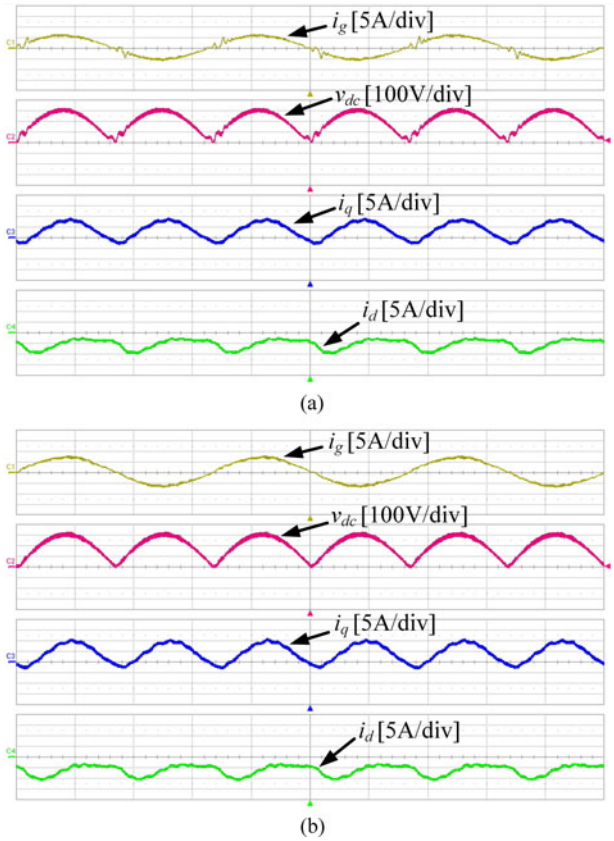

Fig. 11. Waveforms of the motor drive with the proposed current reference generation method and the direct inverter output power control method. (a) Conventional overmodulation method. (b) Proposed overmodulation method.

motor. Since the dc-link voltage fluctuates as the frequency of 120 Hz, the motor currents are not well controlled. Furthermore, the grid input current has harmonics over the limit because the output power of the inverter is not considered.

From Figs. 9 and 10, the performances of the system where the proposed reference generation is added to the conventional controller can be found. Fig. 9(a) shows the error between the motor current and the reference current ($i_d^* - i_d$, $i_q^* - i_q$) while the constant *d–q* current references are generated, and Fig. 9(b) shows the error with the proposed current references. These figures show that the motor current control error of the proposed method is reduced, especially in the low dc-link voltage area. However, the grid current harmonics are still over the limit, as shown in Fig. 10. It is due to the low bandwidth of the current controller and approximation in the current reference calculation. It clearly shows the limit of the grid-input-current-shaping method by motor current manipulation.

Next, the performance with entire proposed controller is verified. Fig. 11(a) shows the waveforms in the conventional overmodulation [35], and Fig. 11(b) shows the results in the proposed overmodulation. It can be seen that the grid current harmonics

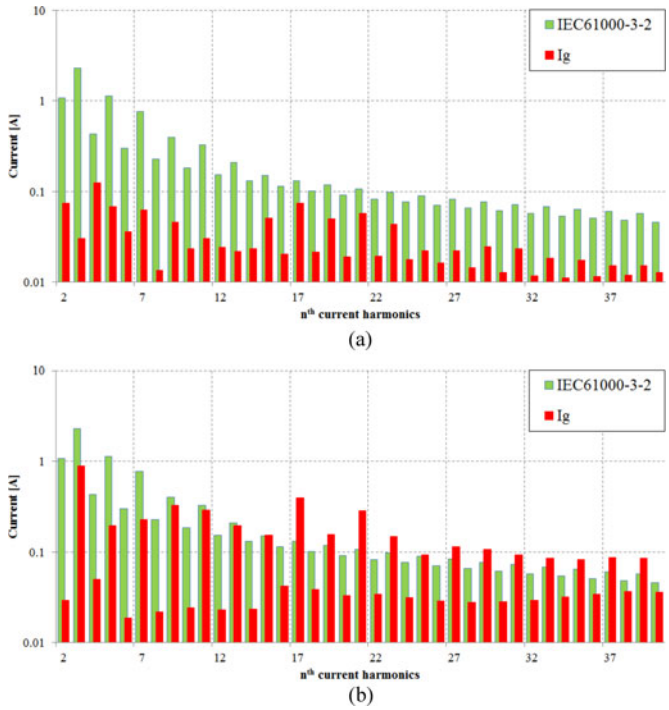

Fig. 12. Grid input current harmonics and the regulation limits. (a) Proposed grid-input-current-shaping method. (b) Grid-input-current-shaping method by manipulating motor current [22].

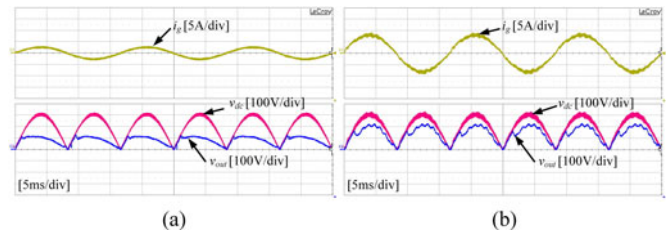

Fig. 13. Output voltage waveform with the proposed grid current shaping method: (a) under low load and (b) under the rated load.

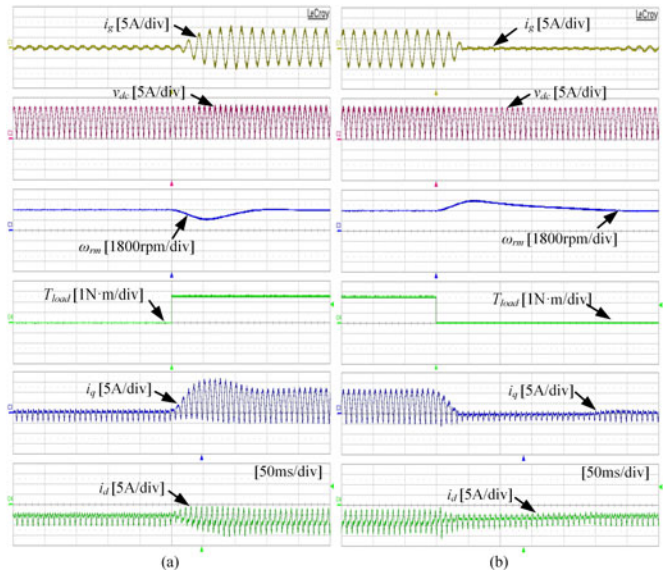

Fig. 14. Step load torque responses of the proposed motor drive: (a) Zero-to-rated torque response. (b) Rated-to-zero torque response.

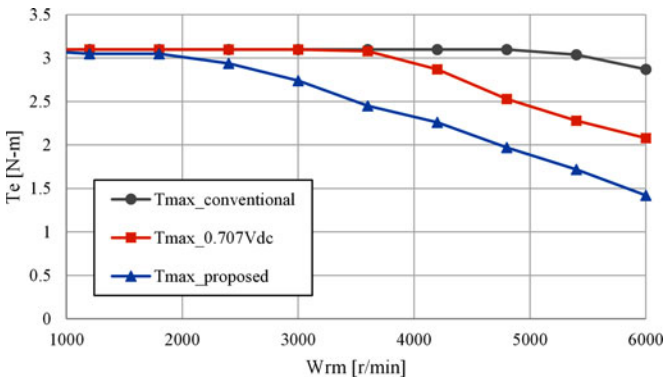

Fig. 15. Capability curve of the motor with the proposed motor drive and with the conventional motor drive.

are significantly reduced. And with the proposed overmodulation method, the grid input current can be shaped even if dc-link voltage is low. Fig. 12(a) and (b) shows the measured amplitudes of the harmonics in the grid input current, compared with the regulation. It can be found that the harmonics with the proposed method are far below the limits. The total harmonic distortion (THD) of the grid input current is 2.52%, and the power factor (PF) of the grid is over 99%. Fig. 13 shows the output voltage waveform with the proposed control method. The output voltage condition (9) is found to be satisfied with the proposed method.

The dynamic load performance of the proposed motor drive is verified by the additional experiment. The zero-to-rated step torque and rated-to-zero torque is applied by the load motor where the speed of the test motor is controlled by the proposed motor drive. Fig. 14(a) and (b) shows the step load performance of the proposed motor drive. The rated-to-zero step response time is about 100 ms longer than the zero-to-rated step response time. It is because minimum torque of the proposed drive system is limited to zero and torque undershoot is blocked. In the proposed system, since a diode rectifier is applied at the grid side and the dc-link capacitance is small, the output torque should be controlled over zero to prohibit the system entering in generating mode and the dc-link voltage rising high.

Finally, the capability curve of the proposed system is measured by the experiment. Because of the small dc-link capacitor, the dc-link voltage in the proposed drive is fluctuating and the average dc-link voltage is reduced to about 0.707 of the voltage in the conventional drive. Also, regular fluctuation of the motor current in the proposed system makes the root-mean-square (rms) motor current higher than the current in the conventional system at the same power point. Due to these reasons, the reduction of the capability curve in the proposed motor drive is inevitable. Fig. 15 shows the capability curves of the conventional drive, the conventional drive with 0.707 of the dc-link voltage and the proposed drive with the same motor. If the thermal margin of the motor is large enough so that current rating

of the proposed system can be designed higher than the rating of the conventional one, capability curve of the proposed drive will be less reduced.

VI. Conclusion

This paper proposed the grid-input-current-shaping method that is applied to the motor drive without electrolytic capacitor. Since dc-link capacitance of the proposed drive system is very small, the waveform of the grid input current is directly affected by the output power of the inverter. Several shaping method were proposed to reduce the harmonics, but the output power of the inverter was not correctly controlled due to the limitations of the controller. To control the output power of the inverter fast and correctly, the grid-input-current-shaping method was proposed in this paper. The current reference generation, the direct output power control by modification of the output voltage reference, and the overmodulation method that maintains the output power of the inverter after the output voltage limitation were included in the proposed method. With the proposed method, the harmonic components of the grid input current can be suppressed under the limits in regulation, without the PFC circuit or the input filter. During the grid input current is shaped, angular speed and torque of the motor also can be regulated. Compared to the conventional motor drive, significant advantage in terms of cost and volume is expected by applying the proposed motor drive.

References

[1] Limits for Harmonic Current Emissions (Equipment Input Current ≤ 16 A Per Phase), IEC 61000-3-2, Part 3-2, Nov. 2005.

[2] W. Chen and S. S. R. Hui, "Elimination of an electrolytic capacitor in AC/DC light-emitting diode (LED) driver with high input power factor and constant output current," *IEEE Trans. Power Electron.*, vol. 27, no. 3, pp. 1598–1607, Mar. 2012.

[3] J. G. Kassakian and T. M. Jahns, "Evolving and emerging applications of power electronics in systems," *IEEE J. Emerg. Sel. Topics Power Electron.*, vol. 1, no. 2, pp. 47–58, Jun. 2013.

[4] J. G. Kim, K. D. Kim, Y. S. Noh, Y. C. Jung, and C. Y. Won, "Analysis and design of a three-port flyback inverter using an active power decoupling method to minimize input capacitance," *J. Power Electron.*, vol. 13, no. 4, pp. 558–568, Jul. 2013.

[5] C. Li, Y. Deng, H. Peng, W. Li, X. He, and Y. Wang, "Partial power conversion device without large electrolytic capacitors for power flow control and voltage compensation," *IEEE Trans. Power Electron.*, vol. 27, no. 12, pp. 4847–4857, Dec. 2012.

[6] H. Ma, J.-S. Lai, Q. Feng, W. Yu, C. Zheng, and Z. Zhao, "A novel valley-fill SEPIC-derived power supply without electrolytic capacitor for LED lighting application," *IEEE Trans. Power Electron.*, vol. 27, no. 6, pp. 3057–3071, Jun. 2012.

[7] G.-S. Seo, K.-C. Lee, and B.-H. Cho, "A new DC anti-islanding technique of electrolytic capacitor-less photovoltaic interface in DC distribution systems," *IEEE Trans. Power Electron.*, vol. 28, no. 4, pp. 4847–4857, Dec. 2012.

[8] A. M. Imam, D. M. Divan, R. G. Harley, and T. G. Habetler, "Real-time condition monitoring of the electrolytic capacitors for power electronics application," in *Proc. IEEE Appl. Power Electron. Conf. Expo.*, Feb. /Mar. 2007, pp. 1057–1061.

[9] D. C. Lee and Y. S. Kim, "Control of single-phase-to-three-phase AC/DC/AC PWM converters for induction motor drives," *IEEE Trans. Ind. Electron.*, vol. 54, no. 2, pp. 797–804, Apr. 2007.

[10] M. Abolhassani, "Modular multipulse rectifier transformers in symmetrical cascaded H-bridge medium voltage drives," *IEEE Trans. Power Electron.*, vol. 27, no. 2, pp. 698–705, Feb. 2012.

[11] A. K. Abdelsalam, M. I. Masoud, M. S. Hamd, and B. W. Williams, "Improved sensorless operation of a CSI-based induction motor drive: Long feeder case," *IEEE Trans. Power Electron.*, vol. 28, no. 8, pp. 4001–4012, Aug. 2013.

[12] H. Akagi and K. Isozaki, "A hybrid active filter for a three-phase 12-pulse diode rectifier used as the front end of a medium-voltage motor drive," *IEEE Trans. Power Electron.*, vol. 27, no. 1, pp. 69–77, Jan. 2012.

[13] S. Wang, X. Ruan, K. Yao, S.-C. Tan, Y. Yang, and Z. Ye, "A flicker-free electrolytic capacitor-less AC–DC LED driver,"*IEEE Trans. Power Electron.*, vol. 27, no. 11, pp. 4540–4548, Nov. 2012.

[14] Y. K. Lo, C. Y. Lin, H. J. Chiu, S. J. Cheng, and J. Y. Lin, "Analysis and design of a push-pull quasi-resonant boost power factor corrector," *IEEE Trans. Power Electron.*, vol. 28, no. 1, pp. 347–356, Jan. 2013.

[15] Y. Cho and J. S. Lai, "Digital plug-in repetitive controller for single-phase bridgeless PFC converters," *IEEE Trans. Power Electron.*, vol. 28, no. 1, pp. 165–175, Jan. 2013.

[16] M. S. Ortmann, S. A. Mussa, and M. L. Heldwein, "Generalized analysis of a multistate switching cells-based single-phase multilevel PFC rectifier," *IEEE Trans. Power Electron.*, vol. 27, no. 1, pp. 46–56, Jan. 2012.

[17] C. Marxgut, F. Krismer, D. Bortis, and J. W. Kolar, "Ultraflat interleaved triangular current mode (TCM) single-phase PFC rectifier," *IEEE Trans. Power Electron.*, vol. 29, no. 2, pp. 873–882, Feb. 2014.

[18] D. Lamar, J. Sebastian, M. Arias, and A. Fernandez, "On the limit of the output capacitor reduction in power-factor correctors by distorting the line input current," *IEEE Trans. Power Electron.*, vol. 27, no. 3, pp. 1168–1176, Mar. 2012.

[19] M. Liserre, F. Blaabjerg, and S. Hansen, "Design and control of an *LCL*-filter-based three-phase active rectifier," *IEEE Trans. Ind. Appl.*, vol. 41, no. 5, pp. 1281–1291, Sep./Oct. 2005.

[20] H. Lamsahel and P. Mutschler, "Permanent magnet drives with reduced DC-link capacitor for home appliances," in *Proc. 35th Annu. Conf. IEEE Ind. Electron.*, 2009, pp. 725–730.

[21] H. S. Jung, S. J. Chee, S. K. Sul, Y. J. Park, H. S. Park, and W. K. Kim, "Control of three-phase inverter for AC motor drive with small DC-link capacitor fed by single-phase AC source," *IEEE Trans. Ind. Appl.*, vol. 50, no. 2, Mar./Apr. 2014.

[22] K. Inazuma, H. Utsugi, K. Ohishi, and H. Haga, "High power factor single-phase diode rectifier driven by repetitively controlled IPM motor," *IEEE Trans. Ind. Electron.*, vol. 60, no. 10, pp. 4427–4437, Oct. 2013.

[23] I. Takahashi and H. Haga, "Direct torque IPM motor control method to obtain unity power factor using a single-phase diode rectifier," in *Proc. IEEE IEMDC*, Jun. 2003, vol. 2, pp. 1078–1083.

[24] W. J. Lee, Y. Son, and J. I. Ha, "Single-phase active power filtering method using diode-rectifier-fed motor drive," in *Proc. IEEE Energy Convers. Congr. Expo.*, 2013, pp. 2461–2465.

[25] M. Hinkkanen and J. Luomi, "Induction motor drives equipped with diode rectifier and small DC-link capacitance," *IEEE Trans. Ind. Electron.*, vol. 55, no. 1, pp. 312–320, Jan. 2008.

[26] A. V. Jouanne, P. N. Enjeti, and B. Banerjee, "Assessment of ride-through alternatives for adjustable-speed drives," *IEEE Trans. Ind. Appl.*, vol. 35, no. 4, pp. 908–916, Jul./Aug. 1999.

[27] L. Moran, P. D. Ziogas, and G. Joos, "Design aspects of synchronous PWM rectifier–inverter systems under unbalanced input voltage conditions," *IEEE Trans. Ind. Appl.*, vol. 28, no. 6, pp. 1286–1293, Nov./Dec. 1992.

[28] M. Liserre, C. Klumper, F. Blaabjerg, V. G. Monopoli, and A. Dell'Aquila, "Evaluation of the ride-through capability of an active-front-end adjustable speed drive under real grid conditions," in *Proc. 30th Annu. Conf. IEEE Ind. Electron.*, 2004, pp. 1688–1693.

[29] H. Fujita, H. Akagi, and Y. Watanabe, "Dynamic control and performance of a unified power flow controller for stabilizing an AC transmission system," *IEEE Trans. Power Electron.*, vol. 21, no. 4, pp. 1013–1020, Jul. 2006.

[30] V. Blasko, V. Kaura, and W. Niewiadomski, "Sampling of discontinuous voltage and current signals in electrical drives : A system approach," *IEEE Trans. Ind. Appl.*, vol. 34, no. 5, pp. 1123–1130, Sep./Oct. 1998.

[31] H. Kim, M. W. Degner, J. M. Guerrero, F. Briz, and R. D. Lorenz, "Discrete-time current regulator design for AC machine drives," *IEEE Trans. Ind. Appl.*, vol. 46, no. 4, pp. 1425–1435, Jul./Aug. 2010.

[32] F. Briz, M. W. Degner, and R. D. Lorenz, "Analysis and design of current regulators using complex vectors," *IEEE Trans. Ind. Appl.*, vol. 36, no. 3, pp. 817–825, May/Jun. 2000.

[33] S. K. Sul, Control of Electric Machine Drive Systems. Hoboken, NJ: Wiley-IEEE Press, 2011, pp. 158–179.

[34] W. J. Lee and S. K. Sul, "DC-link voltage stabilization for reduced DC-link capacitor inverter," *IEEE Trans. Ind. Appl.*, vol. 50, no. 1, pp. 1740–1744, Jan./Feb. 2014.

[35] D. R. Seidl, D. A. Kaiser, and R. D. Lorentz, "One-step optimal space vector PWM current regulation using a neural network," in *Proc. Conf. Rec. IEEE IAS Annu. Meet.*, Denver, CO, USA, Oct. 1994, pp. 867–874.
[36] J. K. Seok, J. S. Kim, and S. K. Sul, "Overmodulation strategy for high-performance torque control," *IEEE Trans. Power Electron.*, vol. 13, no. 4, pp. 786–792, Jul. 1998.
[37] B. H. Bae and S. K. Sul, "A novel dynamic overmodulation strategy for fast torque control of high-saliency-ratio AC motor," *IEEE Trans. Ind. Appl.*, vol. 41, no. 4, pp. 1013–1019, Jul./Aug. 2005.
[38] T. Miyajima, H. Fujimoto, and M. Fujitsuna, "A precise model-based design of voltage phase controller for IPMSM," *IEEE Trans. Power Electron.*, vol. 28, no. 12, pp. 5655–5664, Dec. 2013.
[39] A. Tripathi, A. M. Khambadkone, and S. K. Panda, "Dynamic control of torque in overmodulation and in the field weakening region," *IEEE Trans. Power Electron.*, vol. 21, no. 4, pp. 1091–1098, Jul. 2006.
[40] A. Kwasinski and P. T. Krein, "An integrated 42-V drive design for automobile loads with a low-distortion overmodulation strategy," *IEEE Trans. Power Electron.*, vol. 21, no. 3, pp. 648–658, May 2006.
[41] C. Patel, R. P. P. Day, A. Dey, R. Ramchand, K. K. Gopakumar, and M. P. Kazmierkowski, "Fast direct torque control of an open-end induction motor drive using 12-sided polygonal voltage space vectors," *IEEE Trans. Power Electron.*, vol. 27, no. 1, pp. 400–410, Jan. 2012.
[42] R. Nalepa and T. Orlowska-Kowalska, "Optimum trajectory control of the current vector of a nonsalient-pole PMSM in the field-weakening region," *IEEE Trans. Ind. Electron.*, vol. 59, no. 7, pp. 2867–2876, Jul. 2012.
[43] J. Chen and K. Chin, "Automatic flux-weakening control of permanent magnet synchronous motors using a reduced-order controller," *IEEE Trans. Power Electron.*, vol. 15, no. 5, pp. 881–890, Sep. 2000.
[44] S. Morimoto, M. Sanada, and Y. Takeda, "Wide-speed operation of interior permanent magnet synchronous motors with high-performance current regulator," *IEEE Trans. Ind. Appl.*, vol. 30, no. 4, pp. 920–926, Jul./Aug. 1994.
[45] G. Pellegrino, E. Armando, and P. Guglielmi, "Direct flux field-oriented control of IPM drives with variable dc link in the field-weakening region," *IEEE Trans. Ind. Appl.*, vol. 45, no. 5, pp. 1619–1627, Sep./Oct. 2009.

Yeongrack Son (S'13) was born in Korea, in 1988. He received the B.S. and the M.S. degrees in electrical engineering in 2011 and 2013, respectively, from Seoul National University, Seoul, Korea, where he is currently working toward the Ph.D. degree.

His current research interests include low-cost electric machine drives and the driving structure of the hybrid electric vehicle (HEV).

Jung-Ik Ha (S'97–M'01–SM'12) was born in Korea, in 1971. He received the B.S., M.S., and Ph.D. degrees in electrical engineering from Seoul National University, Seoul, Korea, in 1995, 1997, and 2001, respectively.

From 2001 to 2002, he was a Researcher in Yaskawa Electric Co., Japan. From 2003 to 2008, he was with Samsung Electronics Co., Korea, as a Senior and Principal Engineer. From 2009 to 2010, he was a Chief Technology Officer with LS Mecapion Co., Korea. Since 2010, he has been an Assistant Professor in the Department of Electrical and Computer Engineering, Seoul National University. His current research interests include circuits and control for high-efficiency and integrated electric energy conversions in various industrial fields.